THE JOURNAL OF BIOLOGICAL CHEMISTRY VOL. 283, NO. 40, pp. 27300–27313, October 3, 2008

Tarantula Huwentoxin-IV Inhibits Neuronal Sodium Channels by Binding to Receptor Site 4 and Trapping the Domain II Voltage Sensor in the Closed Configuration*[S]

Received for publication, October 11, 2007, and in revised form, June 11, 2008 Published, JBC Papers in Press, July 14, 2008, DOI 10.1074/jbc.M708447200

Yucheng Xiao[‡§], Jon-Paul Bingham[¶], Weiguo Zhu[‡], Edward Moczydlowski[‖], Songping Liang[§1], and Theodore R. Cummins[‡2]

From the [‡]Department of Pharmacology and Toxicology, Stark Neurosciences Research Institute, Indiana University School of Medicine, Indianapolis, Indiana 46202, [¶]Department of Molecular Biosciences and Bioengineering, University of Hawaii, Honolulu, Hawaii 96822, [‖]Department of Biology, Clarkson University, Potsdam, New York 13699, and [§]Life Sciences College, Hunan Normal University, Changsha, Hunan 410081, China

Peptide toxins with high affinity, divergent pharmacological functions, and isoform-specific selectivity are powerful tools for investigating the structure-function relationships of voltage-gated sodium channels (VGSCs). Although a number of interesting inhibitors have been reported from tarantula venoms, little is known about the mechanism for their interaction with VGSCs. We show that huwentoxin-IV (HWTX-IV), a 35-residue peptide from tarantula *Ornithoctonus huwena* venom, preferentially inhibits neuronal VGSC subtypes rNav1.2, rNav1.3, and hNav1.7 compared with muscle subtypes rNav1.4 and hNav1.5. Of the five VGSCs examined, hNav1.7 was most sensitive to HWTX-IV (IC_{50} ~ 26 nM). Following application of 1 μM HWTX-IV, hNav1.7 currents could only be elicited with extreme depolarizations (>+100 mV). Recovery of hNav1.7 channels from HWTX-IV inhibition could be induced by extreme depolarizations or moderate depolarizations lasting several minutes. Site-directed mutagenesis analysis indicated that the toxin docked at neurotoxin receptor site 4 located at the extracellular S3-S4 linker of domain II. Mutations E818Q and D816N in hNav1.7 decreased toxin affinity for hNav1.7 by ~300-fold, whereas the reverse mutations in rNav1.4 (N655D/Q657E) and the corresponding mutations in hNav1.5 (R812D/S814E) greatly increased the sensitivity of the muscle VGSCs to HWTX-IV. Our data identify a novel mechanism for sodium channel inhibition by tarantula toxins involving binding to neurotoxin receptor site 4. In contrast to scorpion β-toxins that trap the IIS4 voltage sensor in an outward configuration, we propose that HWTX-IV traps the voltage sensor of domain II in the inward, closed configuration.

Voltage-gated sodium channels (VGSCs)[3] are important transmembrane proteins expressed in most excitable tissues. The opening of the pore-forming α subunit is responsible for the rapid depolarizing phase of action potentials. Nine distinct VGSC α subunit subtypes (Nav1.1–1.9) have been cloned from mammals (1, 2). The α subunits share over 75% sequence similarity with each other and often exhibit similar functional properties. Because of these similarities, biological toxins that selectively target VGSC subtypes can be crucial for investigating the distribution and divergent physiological functions of VGSCs.

Many different animals have evolved small molecules or polypeptides that target VGSCs to aid the capture of prey or enhance defenses against predators (3). Investigation of these biological toxins has greatly contributed to our understanding of the physiological roles and structure-function of VGSCs (4). The small molecule VGSC inhibitor tetrodotoxin (TTX) has proven extremely useful, and VGSC subtypes are often classified as TTX-sensitive (Nav1.1–1.4, Nav1.6, and Nav1.7) or TTX-resistant (Nav1.5, Nav1.8, and Nav1.9) (1, 5). Polypeptide toxins can also exhibit high selectivity for VGSC subtypes and, compared with TTX, may have advantages for studying VGSCs. For example, the μ-conotoxin GIIIA potently blocks rat Nav1.4 but has little effect on other subtypes (6, 7), and the tarantula toxin hainantoxin-I inhibits Nav1.2 without affecting sensory neuron VGSCs (8). Animal polypeptide toxins can modulate the activities of sodium channels in diverse manners. More than six toxin receptor sites have been identified or proposed on VGSCs (9, 10). Neurotoxin receptor site 1, located in the outer vestibule of the channel pore, is the site of action for TTX and is often targeted by μ-conotoxins (6). Scorpion α-toxins and sea anemone toxins bind to neurotoxin receptor site 3 at the extracellular S3-S4 linker on domain IV to slow inactivation kinetics (11). Scorpion β-toxins enhance activation by binding to neurotoxin receptor site 4 at the extracellular S3-S4 linker on domain II and trapping the IIS4 voltage sensor in the outward, activated configuration (12).

Over 30 peptide toxins targeting VGSCs have been identified from spider venoms (13). However, little is known

* This work was supported, in whole or in part, by National Institutes of Health Grant NS054642 from the NINDS (to T. R. C. and J. P. B.). This work was also supported by the National Natural Science Foundation of China under Contract 30670640 (to S. L.) and the National 973 Project of China under Contract 2006CB708508 (to Y. X.). Part of this work was presented in abstract form at the Society for Neuroscience Annual Meeting, November 3–7, 2007 in San Diego. The costs of publication of this article were defrayed in part by the payment of page charges. This article must therefore be hereby marked "*advertisement*" in accordance with 18 U.S.C. Section 1734 solely to indicate this fact.

[S] The on-line version of this article (available at http://www.jbc.org) contains supplemental Figs. 1–3 and Table 1.

[1] To whom correspondence may be addressed. E-mail: liangsp@hunnu.edu.cn.

[2] To whom correspondence may be addressed. E-mail: trcummin@iupui.edu.

[3] The abbreviations used are: VGSC, voltage-gated sodium channel; HWTX-IV, huwentoxin-IV; TTX, tetrodotoxin; DRG, dorsal root ganglia; HWTX-I, huwentoxin-I; HEK293, human embryonic kidney 293; WT, wild type.

about the mechanisms of action for inhibitory spider toxins. Huwentoxin-IV (HWTX-IV) is a typical inhibitory cysteine knot peptide from the tarantula *Ornithoctonus huwena* and can inhibit TTX-sensitive VGSCs on adult rat dorsal root ganglia (DRG) neurons (14). In this study, we investigated the toxin sensitivity for Nav1.2, Nav1.3, Nav1.4, Nav1.5, and Nav1.7 and the mechanism of the inhibition by HWTX-IV. Our data indicate that HWTX-IV preferentially blocks peripheral nerve subtype Nav1.7 by binding neurotoxin receptor site 4. Importantly in contrast to scorpion β-toxins, our data suggest that HWTX-IV traps the IIS4 voltage sensor in a closed configuration, therefore providing novel mechanistic insight into the mechanism of action of tarantula toxins that inhibit VGSCs.

EXPERIMENTAL PROCEDURES

Toxin Purification—Huwentoxin-I (HWTX-I) and HWTX-IV were purified from the venom of the female tarantula *O. huwena* as described by Liang *et al.* (15) and Peng *et al.* (14), respectively. The purity of the toxins used in this study was determined to be over 99% by high pressure liquid chromatography and matrix-assisted laser desorption ionization time-of-flight analysis.

Plasmids and Construction of Nav1.4, Nav1.5, and Nav1.7 Mutants—The cDNA genes encoding Nav1.2, Nav1.3, and Nav1.4 from rat were subcloned into the vectors pRC-CMV, pcDNA3.1-mod, and pRBG4, respectively (16–18). The cDNA genes encoding Nav1.5 and Nav1.7 from human were subcloned into the vectors pcDNA3.1 and pcDNA3.1-mod, respectively (19). Auxiliary subunits β1 and β2 both were cloned from human and inserted into an internal ribosome entry site vector (20). All mutations of Nav1.4 (N655D, Q657E, and N655D/Q657E), Nav1.7 (D816N, E818Q, and D816N/E818Q), and Nav1.5 (R812D/S814E) were constructed using the QuikChange II XL Site-Directed Mutagenesis kit according to the manufacture's instruction. The forward and reverse primers with a length of 30 base nucleotides were designed, and only one nucleotide in the code encoding Asp, Asn, Glu, or Gln was replaced (AAT↔ GAT and CAA↔ GAA) with the exception of the R812D and S814E mutations in hNav1.5 where multiple nucleotides were replaced (CGC↔ GAC and AGC↔ GAG). All constructs were sequenced to confirm that the appropriate mutations were made. None of the mutations caused major changes in VGSC gating properties (supplemental Fig. 1 and supplemental Table 1).

Transient Transfection—Transient transfections of Nav1.4, Nav1.5, and Nav1.7 mutant constructs into human embryonic kidney 293 (HEK293) cells were performed using the calcium phosphate precipitation method. HEK293 cells were grown under standard tissue culture conditions (5% CO_2 and 37 °C) in Dulbecco's modified Eagle's medium supplemented with 10% fetal bovine serum. The mutant Nav1.7 channels were cotransfected with the human β1 and β2 subunits (20) to increase the current density, whereas the mutant Nav1.4 and Nav1.5 channels were transfected without any β subunit. The calcium phosphate-DNA mixture (channel constructs and a green fluorescent protein reporter plasmid) was added to the cell culture medium and left for 3 h after which the cells were washed with fresh medium. Cells with green fluorescent protein fluorescence were selected for whole-cell patch clamp recordings 36–72 h after transfection.

Preparation of Stably Transfected Cell Lines—The transfections of all wild type sodium channels (Nav1.2, Nav1.3, Nav1.4, Nav1.5, and Nav1.7) were carried out according to the method as described above, but no green fluorescent protein reporter plasmid was included in the calcium phosphate-DNA mixture. After transfection for 15–20 h, the cells were washed with fresh medium. After 48 h, antibiotic (G418, Geneticin; Cellgro, Herndon, VA) was added to select for neomycin-resistant cells. After 2–3 weeks in G418, colonies were picked, split, and subsequently tested for channel expression using whole-cell patch clamp recording techniques.

Whole-cell Patch Clamp Recordings—Whole-cell patch clamp recordings were performed at room temperature (~21 °C) using an EPC-10 amplifier (HEKA, Lambrecht, Germany). Data were acquired on a Pentium IV computer using the Pulse program (version 8.31; HEKA). Fire-polished electrodes (0.8–1.5 megaohms) were fabricated from 1.7-mm capillary glass (VWR, West Chester, PA) using a P-97 puller (Sutter, Novato, CA). The access resistance ranged from 0.9 to 3.2 megaohms. The standard pipette solution contained 140 mM CsF, 1 mM EGTA, 10 mM NaCl, and 10 mM HEPES, pH 7.3. The standard bathing solution was 140 mM NaCl, 3 mM KCl, 1 mM $MgCl_2$, 1 mM $CaCl_2$, and 10 mM HEPES, pH 7.3. For the experiments described in Fig. 4, modified solutions were used to enhance outward sodium current amplitudes. The modified pipette solution contained 108 mM NaCl, 35 mM CsF, 1 mM EGTA, 2 mM KCl, and 10 mM HEPES, pH 7.3. The modified bathing solution contained 105 mM NaCl, 35 mM *N*-methyl-D-glucamine chloride, 5 mM CsCl, 2 mM KCl, 1 mM $MgCl_2$, 1 mM $CaCl_2$, and 10 mM HEPES, pH 7.3. The liquid junction potential for these solutions was <8 mV; data were not corrected to account for this offset. Voltage errors were minimized using 80% series resistance compensation, and the capacitance artifact was canceled using the computer-controlled circuitry of the patch clamp amplifier. The offset potential was zeroed before patching. After establishing the whole-cell recording configuration, the resting potential was held at −100 mV for 5 min to allow adequate equilibration between the micropipette solution and the cell interior. Linear leak subtraction, based on resistance estimates from four to five hyperpolarizing pulses applied before the depolarizing test potential, was used for all voltage clamp recordings. Membrane currents were usually filtered at 5 kHz and sampled at 20 kHz. For measurement of deactivation kinetics (see Fig. 6), tail currents were filtered at 50 kHz and sampled at 100 kHz.

Toxin Solutions and Bath Application—The stock solution for HWTX-IV at 1 mM was made using double distilled water, and aliquots were stored at −20 °C. Before use, the solution was diluted to the concentrations of interest with fresh bathing solution. Toxin was diluted into the recording chamber (volume of 300 μl) and mixed by repeatedly pipetting 30 μl to achieve the specified final concentration. The mixing proce-

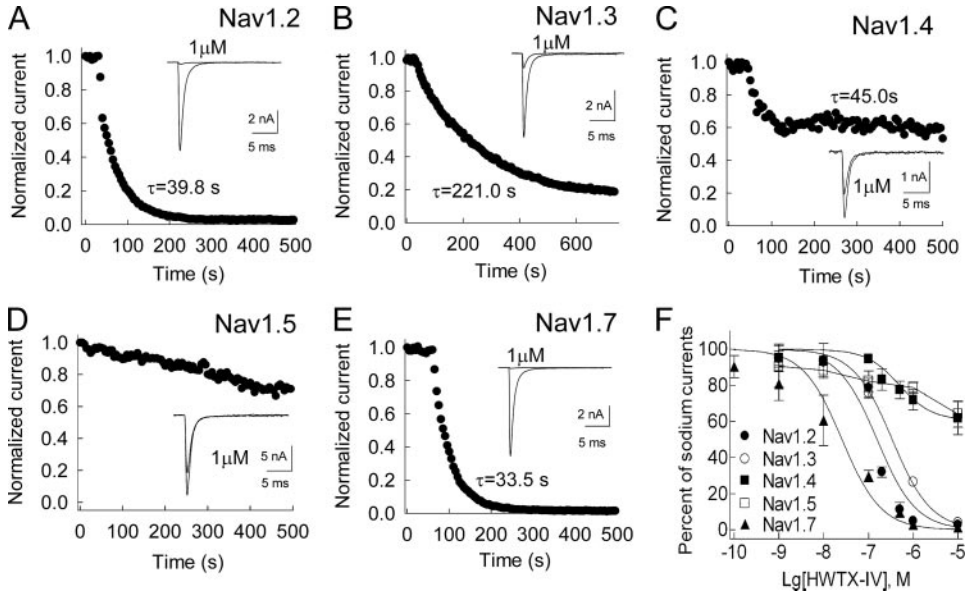

FIGURE 1. **HWTX-IV differentially blocked five WT sodium channel isoforms expressed in HEK293 cells.** Nav1.2 (*A*), Nav1.3 (*B*), and Nav1.4 (*C*) rat sodium channels and Nav1.5 (*D*) and Nav1.7 (*E*) human sodium channels were exposed to HWTX-IV. All inward current traces (*inset*) were elicited by a 20-ms depolarizing potential of −10 mV from a holding potential of −100 mV every 5 s. Data are normalized to the maximum peak current amplitude. After exposure to 1 μM HWTX-IV, inward currents from Nav1.2 and Nav1.7 were inhibited completely (*A* and *E*), and around 80.9% of Nav1.3 current was inhibited (*B*). The time constants of inhibition (*inset*) were ~39.5, 33.5, and 221.0 s, respectively. However, 1 μM HWTX-IV had little effect on Nav1.4 (*C*; $\tau \sim$ 45.0 s) and Nav1.5 (*D*) currents. Note that the inhibitory time constant could not be calculated on Nav1.5. *F*, dose-response inhibitory curves for HWTX-IV on WT Nav1.2, Nav1.3, Nav1.4, Nav1.5, and Nav1.7. Each data point shown as mean ± S.E. comes from three to seven experimental cells. Data points were fitted with the Hill logistic equation as described under "Experimental Procedures." The f_{max} values yielded were 0 on Nav1.2, Nav1.3, and Nav1.7 channels, whereas the value was 59.2% for the Nav1.4 channel. The Hill coefficient was set to 1 for all of the fits to the TTX-sensitive VGSC isoforms. We believe that this is reasonable based on the mutagenesis experiments that indicated that there is one high affinity binding site. For Nav1.4, which exhibited low sensitivity to HWTX-IV, it was estimated to be 0.9. Note that the dose-response curve for Nav1.5 could not be accurately fitted, and therefore the *line* is drawn to connect the data points and guide the eye. Data are mean ± S.E. *Lg*, Log.

dure typically took ~5 s. The extent of the inhibitory effect of toxin was typically assessed around 10–16 min after toxin treatment.

Data Analysis—Data were analyzed using the Pulsefit (HEKA) and Sigmaplot9.0 (Sigma) software programs. All data points are shown as mean ± S.E. *n* is presented as the number of the separate experimental cells. Dose-response curves were fitted using the following Hill logistic equation: $y = 1 - (1 - f_{max})/(1 + ([Tx]/IC_{50})^n)$ where *n* is an empirical Hill coefficient and f_{max} is the fraction of current resistant to inhibition at high toxin (Tx) concentration. The Hill coefficient was set to 1 except where indicated otherwise. This is reasonable based on the results of our mutagenesis data, which indicated a single high affinity binding site for most of the sodium channel isoforms.

RESULTS

Selectivity of HWTX-IV for Sodium Channel Subtypes—Previous work demonstrated that 1 μM HWTX-IV completely inhibits TTX-sensitive sodium currents in adult rat DRG neurons but has no effect on TTX-resistant currents (14); however, the effects of HWTX-IV on specific VGSC isoforms are unclear. Therefore we first investigated the ability of HWTX-IV to block currents generated by five VGSC subtypes (Nav1.2, Nav1.3, Nav1.4, Nav1.5, and Nav1.7) expressed in HEK293 cells. Using whole-cell voltage clamp recording techniques, currents were elicited by a 20-ms depolarizing potential of −10 mV from a holding potential of −100 mV every 5 s. As shown in Fig. 1, toxin treatment differentially caused a time-dependent inhibitory response on the five VGSC subtypes that we tested. We observed that 1 μM HWTX-IV could rapidly and completely decrease current amplitudes for wild type (WT) Nav1.2 ($n = 5$) and Nav1.7 ($n = 6$). The time constants for this inhibition were 39.8 and 33.5 s, respectively (Fig. 1, *A* and *E*). However, the inhibition was much slower for WT Nav1.3 after perfusion of the toxin at the same dose (τ ~221 s), which decreased the Nav1.3 current amplitude by 73.5 ± 1.5% ($n = 7$; Fig. 1*B*). In contrast to these three TTX-sensitive neuronal subtypes, WT Nav1.4 and Nav1.5 seemed to be relatively resistant to HWTX-IV; only 28.1 ± 5.6 and 21.3 ± 3.2% of currents were inhibited in cells expressing WT Nav1.4 channels ($n = 7$) and Nav1.5 channels ($n = 3$) by 1 μM HWTX-IV, respectively (Fig. 1, *C* and *D*). This resistance was confirmed with increased toxin concentration; ~70% of Nav1.4 and Nav1.5 current could still be activated after exposure to 10 μM HWTX-IV (Fig. 1*F*). Fig. 1*F* shows that HWTX-IV inhibited WT VGSC subtypes in a concentration-dependent manner. Hill logistic equation fits to these data estimated that the IC_{50} values were 150, 338, 400, and 26 nM for WT Nav1.2, Nav1.3, Nav1.4, and Nav1.7 channels, respectively. The IC_{50} value for Nav1.5 could not be accurately calculated, but our data indicate that it is >10 μM. It is important to note that although the estimated IC_{50} values for Nav1.3 and Nav1.4 are similar, all three of the TTX-sensitive neuronal VGSCs that we tested were inhibited to a greater extent by HWTX-IV than was Nav1.4 (or Nav1.5). These data indicate that Nav1.7, a peripheral neuronal subtype preferentially expressed in most nociceptive DRG and sympathetic ganglion neurons, is most sensitive to inhibition by HWTX-IV of the five VGSC isoforms examined in this study. The order of VGSC sensitivity to HWTX-IV inhibition was Nav1.7 > Nav1.2 > Nav1.3 ≫ Nav1.4 ≥ Nav1.5.

Effects of Subsaturating Concentrations of HWTX-IV on Activation and Inactivation Properties of WT VGSC Subtypes—We next asked whether HWTX-IV was acting as a simple inhibitor or whether HWTX-IV might also alter channel gating behaviors at concentrations that did not completely inhibit the current. A major effect of animal toxins on VGSCs can be modification of the voltage dependence of channel activation and

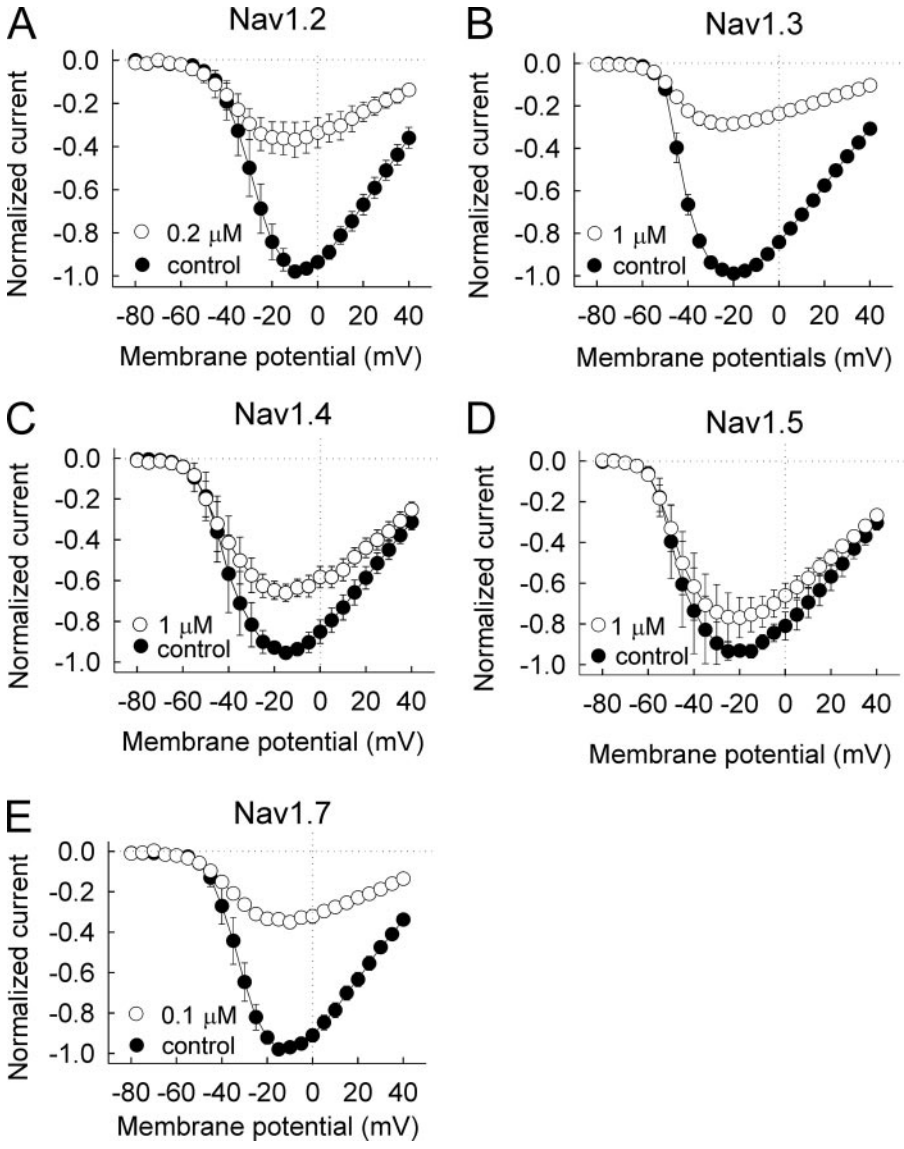

FIGURE 2. **Effects of HWTX-IV on the current-voltage relationships of WT sodium channels.** Cells were held at −100 mV, and families of sodium currents were induced by 50-ms depolarizing steps to various potentials ranging from −80 to +40 mV in 5-mV increments. All currents induced before (*control*) and 10 min after toxin application were normalized to the maximum amplitude of control peak current. Different concentrations of HWTX-IV were applied to Nav1.2 (0.2 μM; *A*), Nav1.3 (1 μM; *B*), Nav1.4 (1 μM; *C*), Nav1.5 (1 μM; *D*), and Nav1.7 (0.1 μM; *E*). Data are mean ± S.E.

inactivation. Many toxins from spiders, such as δ-atracotoxins; Magi5; CcoTx1, CcoTx2, and CcoTx3; PaurTx3; and ProTx-II, are able to shift the threshold of sodium channel activation to more negative or positive potentials (21–26). Therefore we investigated the effects of subsaturating toxin concentrations on the voltage dependence of current activation. The current-voltage relationships were determined for Nav1.2, Nav1.3, Nav1.4, Nav1.5, and Nav1.7 channels using step depolarization ranging from −80 to 40 mV from a holding potential of −100 mV. Fig. 2 shows that under control conditions the threshold of initial channel activation ranged between −65 and −50 mV and that the largest peak current was evoked between −20 and −10 mV. In the presence of HWTX-IV at 0.1, 0.2, or 1 μM, Nav1.7, Nav1.2, and Nav1.3 currents activated between −50 mV and +40 mV were significantly inhibited (Fig. 2, *A*, *B*, and *E*), but only slight inhibitions were detected on Nav1.4 and Nav1.5 after exposure to the toxin at 1 μM (Fig. 2, *C* and *D*). In contrast to ProTx-II and Magi5 (21, 24), HWTX-IV did not modify the threshold of initial channel activation on the five tested VGSC subtypes. Because the toxin had relatively little effect on Nav1.4 and Nav1.5 channels (Figs. 1 and 2), we chose WT neuronal VGSCs (Nav1.2, Nav1.3, and Nav1.7) for further analysis of the effects of HWTX-IV on the voltage dependence of activation and inactivation. As shown in Fig. 3, when channel conductance calculated as described in the figure illustration was normalized, Boltzmann fits indicated that the midpoints of channel activation were −27.8 ± 1.9 and −31.9 ± 1.2 mV for WT Nav1.2 before and after exposure to 0.2 μM toxin (Fig. 3*A*; $n = 3$), −43.2 ± 1.0 and −41.8 ± 0.8 mV for WT Nav1.3 before and after exposure to 1 μM toxin (Fig. 3*B*; $n = 4$), and −31.0 ± 1.0 and −32.7 ± 0.7 mV for WT Nav1.7 before and after exposure to 0.1 μM toxin (Fig. 3*C*; $n = 4$), respectively. These differences were not statistically significant, and no changes were observed in the slope values for the voltage dependence of activation either (data not shown). In contrast to ProTx-II, which does alter the voltage dependence of activation for Nav1.5 and Nav1.7 within the physiological voltage range (24) and the ceratotoxins (CcoTx1, CcoTx2, and CcoTx3) and PaurTx3, which positively shift the voltage dependence of activation of Nav1.2, Nav1.3, and Nav1.4 by 5–20 mV at concentrations that do not fully inhibit the channels (26), these data show that subsaturating concentrations of HWTX-IV have little or no effect on the voltage dependence of activation for the residual current.

We also asked whether subsaturating concentrations of HWTX-IV altered the voltage dependence of steady-state inactivation. Steady-state inactivation is another important property of VGSCs that can modulate the excitability of neurons (27), can be modified by scorpion and spider toxins (28), and contributes to the inhibitory action of therapeutic agents such as lidocaine. Therefore we investigated the effect of HWTX-IV on steady-state inactivation of neuronal VGSC isoforms (WT Nav1.2, Nav1.3, and Nav1.7) using a standard two-pulse protocol. As illustrated in Fig. 3, under control conditions the estimated midpoints of steady-state inactivation were −75.3 ± 0.6, −86.8 ± 0.6, and −75.5 ± 1.8 mV on Nav1.2, Nav1.3, and

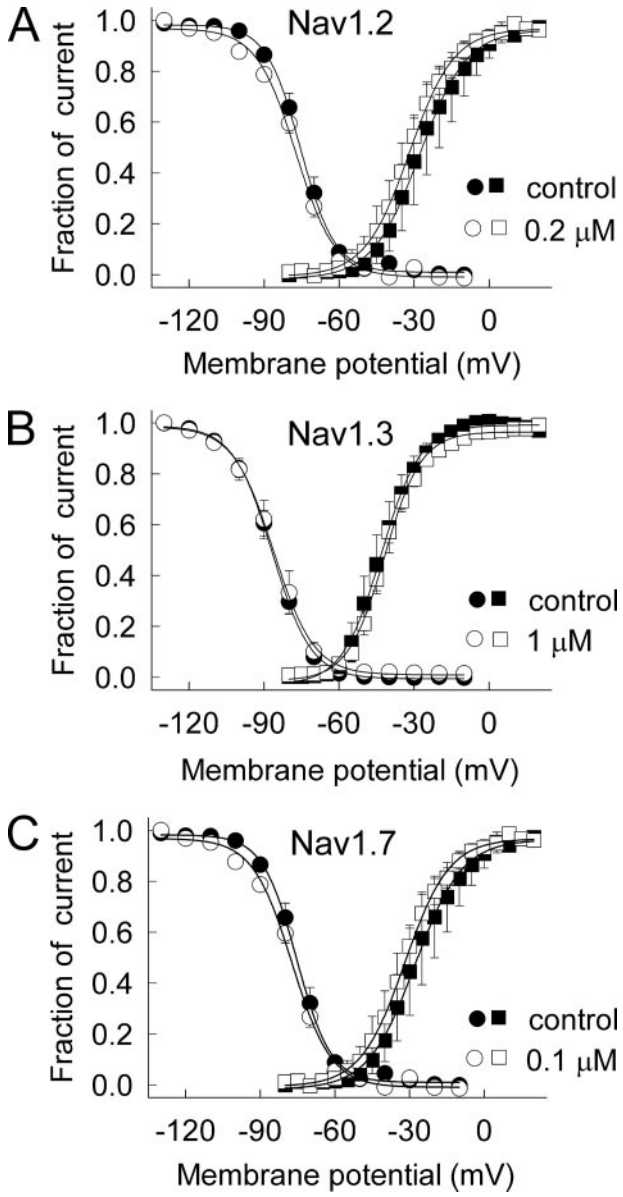

FIGURE 3. **HWTX-IV had no obvious effects on the steady-state activation and inactivation voltage dependence of WT Nav1.2 (*A*), Nav1.3 (*B*) and Nav1.7 (*C*).** Steady-state activation kinetics was estimated based on the data from Fig. 2. The conductance was calculated using the equation $G(\mathrm{Nav}) = I/(V - V_{rev})$ in which I, V, and V_{rev} represent inward current value, membrane potential, and reversal potential, respectively. Data are plotted as a fraction of the maximum conductance. The voltage dependence of steady-state inactivation was estimated using a standard double pulse protocol in which sodium currents were induced by a 20-ms depolarizing potential of −10 mV following a 500-ms prepulse at potentials that ranged from −130 to −10 mV with a 10-mV increment. Cells were held at −100 mV. Currents were plotted as a fraction of the maximum peak current. Data points (mean ± S.E.) for both activation and inactivation kinetics were well fitted with the Boltzmann equation.

Nav1.7, respectively. After toxin treatment (0.2, 1, or 0.1 μM) for ~13 min, the estimated midpoint values were −77.4 ± 0.6, −86.5 ± 1.0, and −72.2 ± 1.3 mV, respectively (n = 3–4). These differences were not statistically significant. Thus, these data indicate that subsaturating concentrations of HWTX-IV have little or no effect on steady-state inactivation of the residual currents conducted by neuronal VGSCs.

The kinetics of activation and inactivation for the residual currents in subsaturating concentrations of HWTX-IV were similar to those of controls on the VGSC subtypes that were tested (data not shown), consistent with previous observations on rat DRG neurons (14). The fact that the kinetics and voltage dependence of residual macroscopic currents in the presence of subsaturating HWTX-IV are virtually identical to the behavior of control currents in the absence of toxin implies that the residual current is simply due to normal channels not occupied by toxin. In other words, the fraction of toxin-occupied channels is electrically silent in this assay. Thus, at first glance, in the physiologically relevant voltage range of −80 to +60 mV, HWTX-IV appears to act as a simple inhibitor or channel blocker in the manner of TTX.

HWTX-IV Is Not a Simple Pore Blocker—The apparent lack of effect of subsaturating concentrations of HWTX-IV on the activation and inactivation properties is consistent with the original proposal that HWTX-IV might interact with neurotoxin receptor site 1 (14). Therefore we tested whether HWTX-IV inhibition was altered by mutation of a pore residue in voltage-gated sodium channels that is critical for binding of toxins to neurotoxin site 1 such as TTX (27) as well as binding of another pore blocker, the μ-conotoxin GIIIB, to Nav1.4 (data not shown). The Y362S mutation in Nav1.7 greatly decreased sensitivity to TTX but did not alter inhibition by HWTX-IV (supplemental Fig. 2). This indicates that HWTX-IV is unlikely to interact with site 1.

The lack of effect of the Y632S mutation on HWTX-IV inhibition raised the possibility that HWTX-IV might not be a simple pore blocker. There is substantial evidence showing that several peptide toxins that inhibit voltage-gated potassium and calcium currents do so by trapping one or more of the voltage sensors in the closed configuration (29–31). The inhibitory action of these potassium and calcium channel inhibitors can be overcome or reversed with large depolarizations, indicating state-dependent binding. Therefore we tested whether Nav1.7 currents could be elicited by strong depolarizations in the presence of a saturating concentration (1 μM) of HWTX-IV.

Cells were depolarized from −80 mV to potentials ranging from −60 to +160 mV in 5-mV increments (Fig. 4, *A*–*C*). Because the sodium currents reversed around +65 mV when recordings were obtained with our standard bath and pipette solutions, we modified the solutions (see "Experimental Procedures") to shift the reversal potential close to 0 mV and enhance the amplitude of the outward sodium currents elicited with strong depolarizations (Fig. 4*A*). As has been observed previously with Nav1.4 channels expressed in HEK293 cells (32), the amplitude of these currents plateaued above 100 mV. This is likely because of the action of cytoplasmic polyamines (32). In the presence of saturating concentrations of HWTX-IV, outward currents can be observed at voltages above 70 mV. At +160 mV, the amplitude of these currents was one-fifth of the current amplitude elicited before toxin application (Fig. 4, *B* and *C*). In five of the toxin-treated cells, we were able to record outward sodium currents in the presence of HWTX-IV with depolarizations extending up to 280 mV (Fig. 4*D*). The data from these cells were compared with data obtained at the same time point (20 min after establishing the whole-cell configuration) from a separate group of control cells. For this comparison, the amplitude of the currents recorded from the control

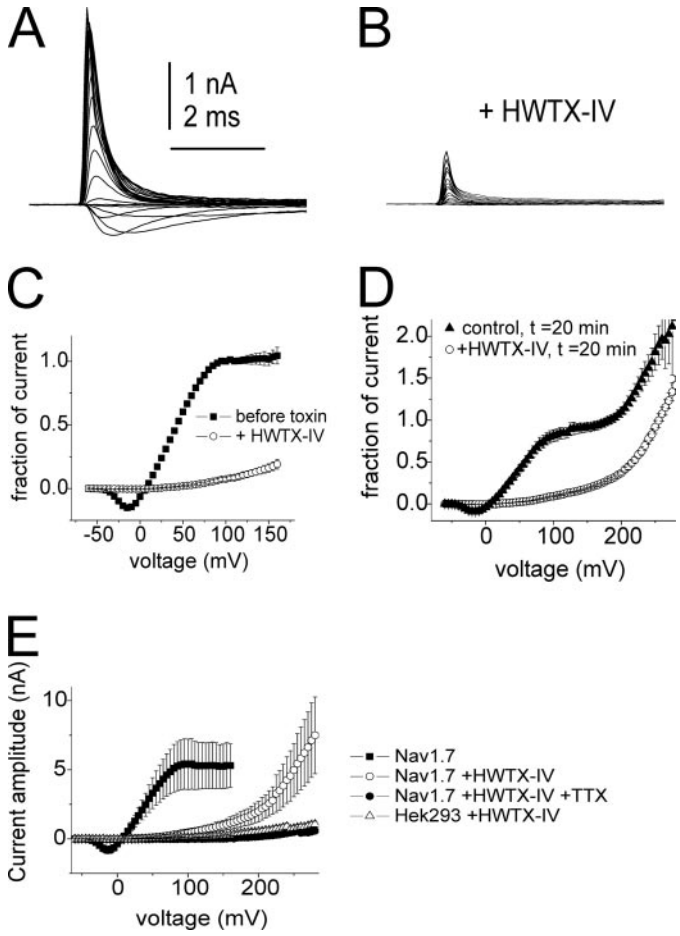

FIGURE 4. **Very large depolarizations can partially activate Nav1.7 channels blocked by HWTX-IV.** Nav1.7 currents were recorded using modified solutions with nearly symmetrical sodium concentrations to enhance the amplitude of outward sodium currents. *A*, Nav1.7 currents recorded from a HEK293 cell expressing Nav1.7 channels just before toxin application ~10 min after establishing the whole-cell recording configuration. The depolarizing voltage steps ranged from −60 to +160 mV. *B*, Nav1.7 currents recorded from the same cell as in *A* following application of 1 μM HWTX-IV. Recording was obtained ~20 min after establishing the whole-cell configuration. *C*, current-voltage plot of peak current amplitude obtained from six cells expressing Nav1.7 channels before and after toxin application (as described for the cell in *A* and *B*). Current amplitudes were normalized to the amplitude recorded at +100 mV before toxin application. *D*, the current-voltage relationship for Nav1.7 obtained from eight control Nav1.7 cells (no toxin) at ~20 min after establishing the whole-cell configuration is compared with data from five of the toxin-treated cells from *C*. In both cases the current amplitudes were normalized to the amplitude recorded at +100 mV in the absence of toxin ~10 min after establishing the whole-cell configuration. This controls for time-dependent changes that might affect the comparison. Cells were depolarized to voltages ranging from −60 mV to +280 mV. *E*, the mean peak current amplitude evoked with different voltage pulses from Nav1.7-expressing HEK293 cells is shown before toxin treatment (*filled squares*), after addition of 1 μM HWTX-IV (*open circles*), and after the subsequent addition of 500 nM TTX (*filled circles*; $n = 3$). For comparison, peak current amplitudes evoked in the presence of 1 μM HWTX-IV from HEK293 cells that did not express recombinant sodium channels is also shown (*open triangles*; $n = 6$), confirming that the outward currents evoked from Nav1.7-expressing HEK293 cells in the presence of HWTX-IV are generated by Nav1.7 channels. Data are mean ± S.E.

cells was normalized to the amplitude obtained with the depolarization to 100 mV. The amplitude of the current recorded from the toxin-treated cells was normalized to the current amplitude obtained before toxin application with the depolarization to 100 mV (as was done for Fig. 4*C*). As can be seen in Fig. 4*D*, at 250 mV the normalized amplitude of the current recorded from the toxin treated cells is approximately half the normalized amplitude of the current recorded from the control cells. It is important to note that the currents activated with extreme depolarizations activated within 1 ms (Fig. 4*B*). To confirm that these currents were indeed produced by the transfected Nav1.7 channels, in three of the toxin-treated cells we applied 500 nM TTX and ran the protocol with the extreme depolarizations again. Fig. 4*E* shows the average current amplitudes of Nav1.7-expressing HEK293 cells before HWTX-IV treatment, after the addition of HWTX-IV, and then after addition of TTX. Current amplitude data obtained with the same voltage protocol from control HEK293 cells that did not express VGSC currents following HWTX-IV treatment but without TTX treatment are also shown. These data show that 1) outward currents elicited by HWTX-IV in HEK293 cells expressing Nav1.7 are blocked by TTX and that 2) similar currents are not observed in HEK293 cells that do not express recombinant VGSCs. Therefore these data show that very large depolarizations can elicit Nav1.7 currents in the presence of HWTX-IV concentrations that completely block currents within the physiological voltage range, indicating that HWTX-IV exhibits voltage-dependent or state-dependent inhibition of VGSCs.

We next asked whether the inhibition of Nav1.7 by HWTX-IV could be altered by repetitive depolarizations and/or prolonged depolarizations. We first examined the kinetics for onset of toxin inhibition with low frequency activity and compared this with inhibition of channels that were not activated until at least 2 min after toxin application (Fig. 5*A*). Inhibition of Nav1.7 was almost independent of pulse frequency. During exposure to 1 μM HWTX-IV, the time constants for inhibition of Nav1.7 were ~33.5 s at 0.2 Hz, ~33.5 s at 0.1 Hz, and ~36.1 s at 0.05 Hz. Importantly inhibition was nearly identical when Nav1.7 current was first activated 130 s after exposure to toxin (Fig. 5*A*). These data show that channel activation is not a requirement for HWTX-IV inhibition. In a second set of experiments we investigated whether prolonged depolarizations could reverse the inhibitory effect of HWTX-IV on Nav1.7. Cells were depolarized to either +30 or +100 mV for 500 ms and then hyperpolarized to −100 mV for 40 ms to allow channels to recover from fast inactivation before the test depolarization to determine the fraction of channels available for activation. Although a significant amount of current was available for activation at the end of this protocol under control conditions, following application of 1 μM HWTX-IV the Nav1.7 channels did not conduct sodium current when a 500-ms depolarizing pulse at +30 or +100 mV was applied (Fig. 5, *B* and *C*; $n = 6$). However, following a 5-min depolarizing pulse at +30 mV ~50% of the Nav1.7 current recovered from HWTX-IV inhibition (Fig. 5*D*; $n = 3$). In this case a 2-s hyperpolarizing pulse was used to allow recovery from both fast and slow inactivation before the final test pulse. These data show that very prolonged depolarizations can reverse the inhibitory effect of HWTX-IV.

Although it was not feasible to accurately determine the time course for reversal at +30 mV, we were able to estimate the time courses for reversal of inhibition at more extreme voltages (Fig. 5*E*). For this set of experiments Nav1.7 channels, in the presence of 1 μM HWTX-IV, were depolarized to +250, +200,

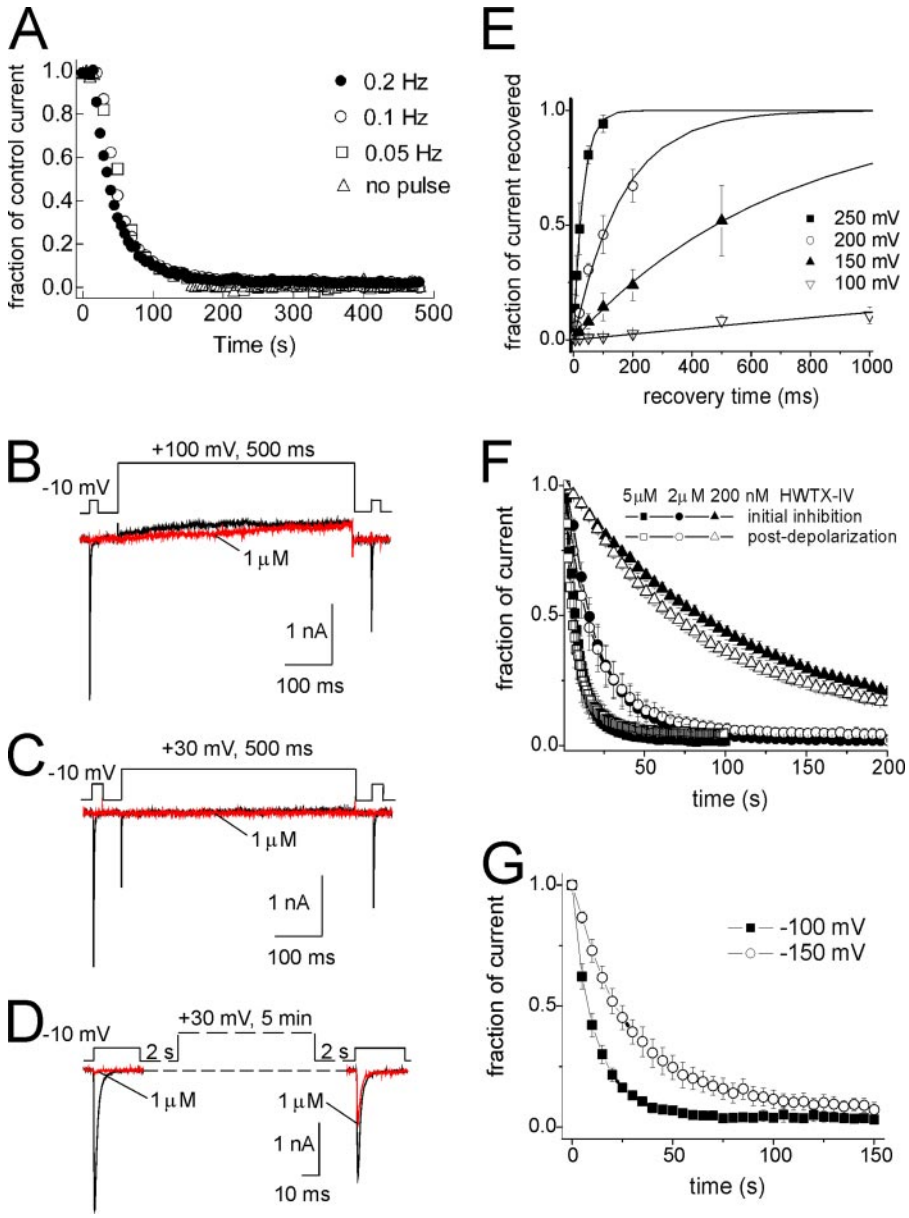

FIGURE 5. **Effect of activation on HWTX-IV inhibition.** *A*, HWTX-IV inhibition is not altered by the rate of channel activation. The time constant for inhibition by 1 μM HWTX-IV with different pulse frequencies is shown. Sodium currents were induced by 20-ms depolarizing potentials of −10 mV from a holding potential of −100 mV. When fitted to single exponential function, the time constants (τ) were ~33.5 s at 0.2 Hz, ~33.5 s at 0.1 Hz, and ~36.1 s at 0.05 Hz. *no pulse* indicates that no pulse was applied for the first 130 s after toxin treatment. Note that in the absence of depolarizing pulses HWTX-IV is still able to block Nav1.7 channels. *B–D*, prolonged or extreme depolarizations allow partial recovery of current from HWTX-IV inhibition. A 500-ms depolarization to either +100 mV (*B*) or +30 mV (*C*) did not promote recovery of Nav1.7 current from block by 1 μM HWTX-IV. Currents were recorded before (*black trace*) and after (*red trace*) HWTX-IV application. Current traces were induced by a three-pulse voltage protocol in which the holding potential was −100 mV and test pulses before and after the 500-ms prolonged depolarizations were 20-ms depolarizations to −10 mV. The interval at −100 mV between each of the three depolarizing pulses was 40 ms, allowing channels to recover from fast inactivation induced by the 500-ms depolarizing pulse. *D*, a 5-min depolarization to +30 mV allows ~50% of the Nav1.7 current to recover from HWTX-IV inhibition. For this protocol a 2-s interval at −100 mV was used before and after the 5-min prolonged depolarization. This allows for recovery from both fast and slow inactivation induced by the prolonged depolarization. *E*, time course for recovery of current following strong depolarizations in the presence of 1 μM HWTX-IV. Current amplitude was measured at −10 mV. Cells were depolarized to +250 (*filled squares*; $n = 3$), +200 (*open circles*; $n = 3$), +150 (*filled triangles*; $n = 4$), and +100 mV (*open inverted triangles*; $n = 5$) for various durations followed by a ~700-ms hyperpolarization to −120 mV (to remove fast inactivation) before testing current available at −10 mV. *F*, comparison of time course for current inhibition following initial application of HWTX-IV (*filled symbols*) and reinhibition following depolarization-induced recovery of current (*open symbols*). The time courses of inhibition were compared for 200 nM (*triangles*; $n = 3$), 2 μM (*circles*; $n = 4$), and 5 μM (*squares*; $n = 3$) HWTX-IV. Current recovery was elicited with a 200-ms depolarization to +250 mV. *G*, the time course for reinhibition is faster at −100 mV (*filled squares*) than at −150 mV (*open circles*). Following application of 1 μM HWTX-IV, cells ($n = 3$) were depolarized to +250 mV for 200 ms then hyperpolarized to −100 or −150 mV. The time course for reinhibition was measured by pulsing to −10 mV for 10 ms once every 5 s. Data are mean ± S.E.

+150, and +100 mV for various durations lasting between 1 and 1000 ms and repolarized to −120 mV for ~700 ms before testing for recovery of Nav1.7 current with a test pulse to −10 mV. In the absence of extreme depolarizations ~98% of Nav1.7 current elicited with a −10-mV depolarization was inhibited by 1 μM HWTX-IV. Depolarizations to +250 mV induced rapid recovery of the current available at −10 mV with a time constant of ~31 ms. Recovery kinetics were very dependent on voltage with the time constant increasing to ~165 ms at +200 mV, ~688 ms at +150 mV, and ~8000 ms at +100 mV (Fig. 5*E*).

These data indicate that extreme, prolonged depolarizations cause HWTX-IV to dissociate from the sodium channel. To determine whether this is likely, we measured the initial time course for inhibition following bath application of 200 nM, 2 μM, and 5 μM HWTX-IV and compared this with the time course for reinhibition of Nav1.7 currents following recovery induced by a 200-ms depolarization to +250 mV (Fig. 5*F*). The time constant for the initial inhibition was 119 ± 11 s with 200 nM HWTX-IV ($n = 3$), 23 ± 5 s with 2 μM HWTX-IV ($n = 4$), and 9.5 ± 1.5 s with 5 μM HWTX-IV ($n = 3$). The time constant for the reinhibition following recovery induced by the extreme depolarization was 84 ± 7 s with 200 nM HWTX-IV ($n = 3$), 20 ± 4 s with 2 μM HWTX-IV ($n = 4$), and 8.1 ± 2.7 s with 5 μM HWTX-IV ($n = 3$). Although the time courses for inhibition were concentration-dependent, at a given concentration the time course for the initial inhibition and the reinhibition were not statistically different, indicating that prolonged depolarizations cause HWTX-IV to dissociate from Nav1.7.

Two distinct mechanisms could explain the ability of extreme depolarizations to induce Nav1.7 current activation and promote dissociation of the toxin from its site of action. HWTX-IV binding to VGSCs might

be state-dependent and depend on the configuration of the channel. Alternatively because HWTX-IV has a net positive charge, association and dissociation of the toxin to the channel could simply be electrogenic or under the direct influence of voltage acting on charged residue(s) of the toxin moving in the electric field. Several lines of evidence support the first mechanism. For one, the rate of reinhibition for 1 μM HWTX-IV was slower at −150 mV than at −100 mV (Fig. 5*G*; $p < 0.05$). If toxin association were purely electrogenic, the rate of reinhibition should be faster at −150 mV, not slower. The simplest explanation for the slower rate at −150 mV is that the configuration of the toxin binding site is voltage-dependent and is not only less favorable at extreme depolarized voltages but is also less favorable at extreme hyperpolarizations as if binding of the toxin is sensitive to the exact displacement of a voltage sensor domain that varies its disposition across the membrane with transmembrane voltage. The second line of evidence that argues against the voltage dependence of toxin inhibition resulting simply from electrogenic interactions is that although very short depolarizations can activate Nav1.7 currents at +200 and +250 mV recovery of the current available at −10 mV required much longer depolarizations at +200 and +250 mV. For example, although in the presence of 1 μM HWTX-IV a single 1-ms depolarization to +250 mV activated 43 ± 3% of the current activated under control conditions at +250 mV, this 1-ms extreme depolarization only allowed recovery of 1.1 ± 0.7% of the current activated at −10 mV. This indicates that channels can activate after toxin inhibition in response to very brief extreme depolarizations, depolarizations that are too brief to allow substantial toxin dissociation.

This was confirmed by analysis of current deactivation kinetics as shown for hanatoxin and Kv2.1 (33). If toxin must dissociate from the channel before current activation, then the deactivation kinetics (the rate at which current decays or channels close in response to repolarization of the membrane potential) following extreme depolarizations should be the same in the presence of toxin and under control conditions. However, if extreme depolarization induces channel activation with the toxin bound, then the deactivation kinetics following short activating pulses should be altered compared with the kinetics under control conditions. We examined the time course for Nav1.7 current deactivation following 0.2-ms depolarizations to 250 mV (Fig. 6). The peak current elicited with the short depolarizations in the presence of 1 μM HWTX-IV (Fig. 6*A*) was ~40% of that elicited under control conditions (compared with only 2% activated with depolarizations to −10 mV). The relative amplitude of the tail current elicited by the repolarizing potential following the short depolarizing pulse was reduced in the presence of HWTX-IV (Fig. 6*B*), indicating rapid closure of channels during the repolarizing transition. The time course for decay (deactivation) of the tail currents in the presence of HWTX-IV was also much faster (Fig. 6, *B* (*inset*) and *C*). The significantly faster deactivation kinetics observed in the presence of HWTX-IV indicates that Nav1.7 channels activate at extreme voltages with toxin bound. If toxin affinity is higher for resting channels, toxin-bound channels should deactivate or return to the resting configuration more rapidly, and prolonged activation, which keeps the channels in a configuration with lower toxin affinity, should promote toxin dissociation. This

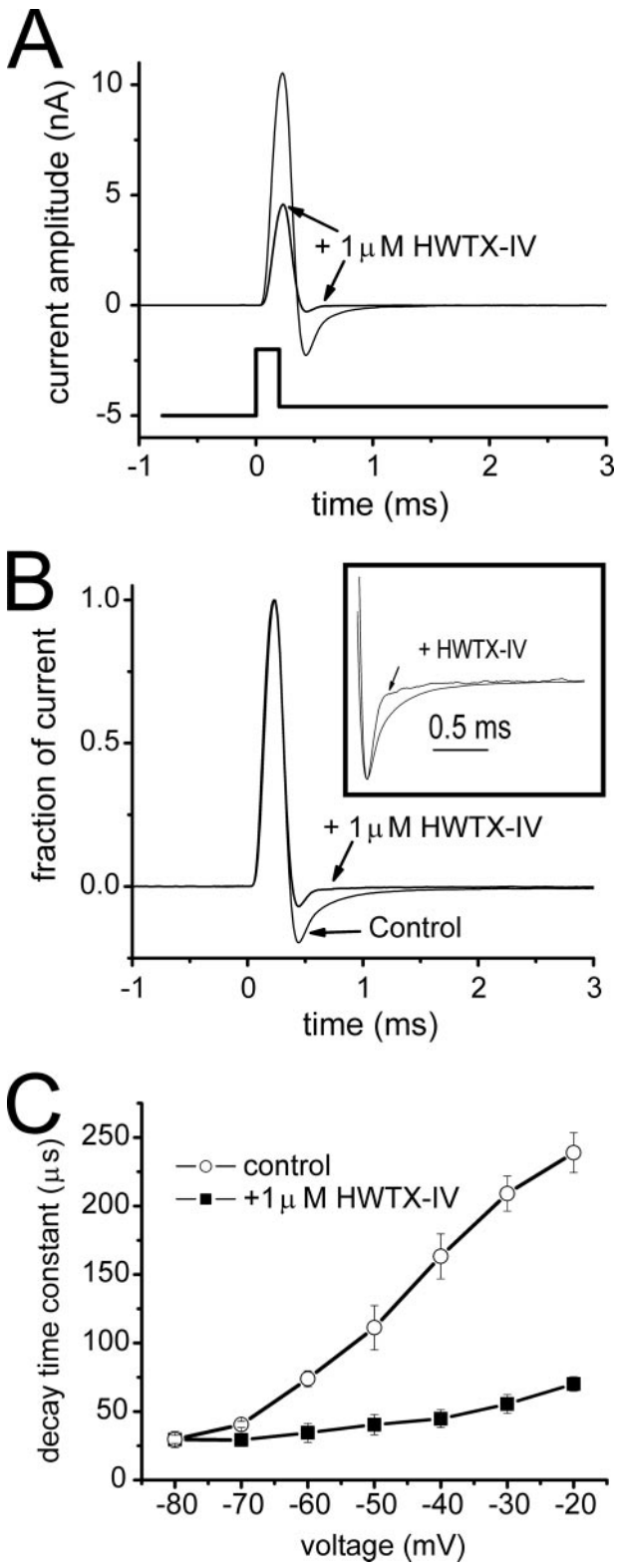

FIGURE 6. **HWTX-IV increases Nav1.7 deactivation following extreme depolarizations.** *A*, current, activated with a 0.2-ms depolarization to +250 mV followed by a repolarization to −40 mV to elicit the tail current, was recorded before and after application of 1 μM HWTX-IV. *B*, the currents shown in *A* are shown normalized to the maximum current elicited during the depolarization. The relative amplitude of the tail current is smaller after exposure to HWTX-IV. The *inset* shows just the tail currents after normalization of the maximum tail current amplitude. The decay of the tail currents is faster after exposure to HWTX-IV. *C*, time constants for tail current decay was measured at voltages between −20 and −80 mV before and after exposure to 1 μM HWTX-IV ($n = 3$). Data are mean ± S.E.

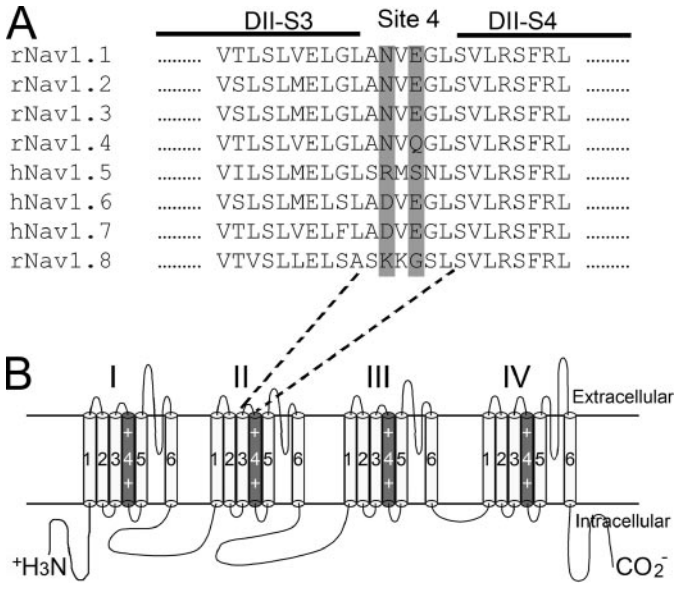

FIGURE 7. **Amino acid sequence alignment of receptor site 4 on sodium channel isoforms.** *A*, crucial determinants of neurotoxin receptor site 4 shown are located at the S3-S4 linker of sodium channel domain II. The positions of amino acids of interest are shaded in *gray*. Nav1.1–1.4 and Nav1.8 channels are from rat (*r*), and Nav1.5–1.7 channels are from human (*h*). *B*, schematic diagram of sodium channel α subunit. The voltage sensor (segment 4) of each domain is shaded in *gray* and marked with "+ +." The sequences of the S3-S4 linker of domain II is indicated in *A*. Nav1.9 is not shown as the IIS3-S4 linker is longer and completely divergent.

is precisely what was observed. These data suggest that HWTX-IV binds to a part of the channel that changes configuration in response to changes in voltage and channel activation, such as the external parts of the voltage sensors of Nav1.7.

Nav1.4, Nav1.5, and Nav1.7 IIS3-S4 Residues Determine Sensitivity to HWTX-IV—Our next goal was to identify the specific residues that determined the sensitivity of VGSCs to HWTX-IV. Many of the toxins that modify activation or inactivation of voltage-gated ion channels bind to the S3-S4 region(s) of the channels (10, 34) that are probably the most external parts of the voltage sensors on voltage-gated ion channels. Although several tarantula toxins that inhibit activation of potassium channels interact with the S3-S4 region, it is not known whether tarantula toxins that inhibit sodium channel activity interact with S3-S4 regions. However, α-scorpion toxins that inhibit sodium channel inactivation interact with the IVS3-S4 linker (neurotoxin site 3) (10, 35), and β-scorpion toxins that enhance sodium channel activation interact with the IIS3-S4 linker (neurotoxin site 4), trapping the voltage sensor of domain II in the open configuration (10). We asked whether HWTX-IV might inhibit activation of TTX-sensitive neuronal sodium channels by interacting with the IIS3-S4 linker. This possibility was supported by sequence alignment of IIS3-S4 linkers (Fig. 7) that shows that an acidic residue (Glu) is conserved in the HWTX-IV-sensitive channel subtypes but not in Nav1.4, Nav1.5, and the neuronal TTX-resistant channels. Acidic residues are often involved in toxin binding (10), and HWTX-IV has a net positive charge. A second acidic residue (Asp) is present only in the IIS3-S4 linkers of the Nav1.6 and Nav1.7 subtypes. To investigate the role of the two acidic residues in binding HWTX-IV, we constructed three mutants of Nav1.4

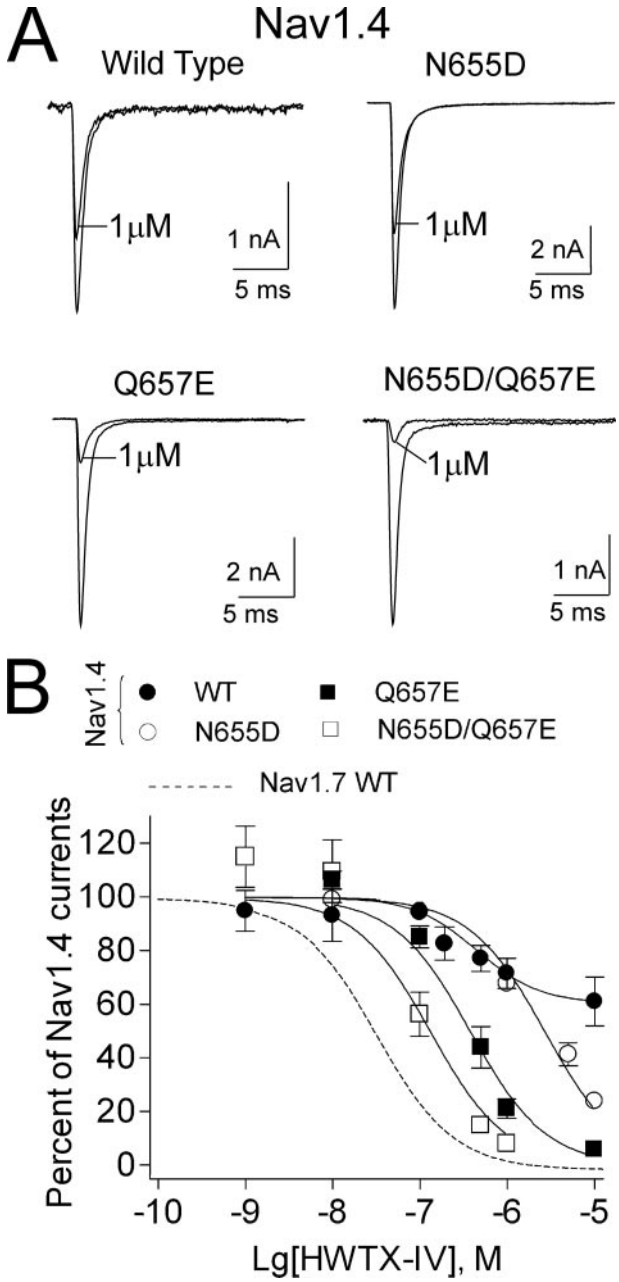

FIGURE 8. **Effects of HWTX-IV on WT and mutant Nav1.4 channels expressed in HEK293 cells.** *A*, representative current traces for wild type and mutant (N655D, Q657E, and N655D/Q657E) Nav1.4 channels were elicited by depolarization to −10 mV from a holding potential of −100 mV. The toxin concentration was 1 μM. *B*, dose-response inhibitory curves of HWTX-IV on WT and mutant Nav1.4 channels. Data points (mean ± S.E., each from three to five experimental cells) were fitted according to the standard Hill equation as described under "Experimental Procedures." The f_{max} values were 0 for all Nav1.4 mutants tested. The *dashed line* shows the fitted dose-response curve for toxin inhibition of WT Nav1.7 (see Fig. 1*F*). *Lg*, Log.

(N655D, Q657E, and N655D/Q657E) using a site-directed mutagenesis technique where the residues in Nav1.4 were replaced with the corresponding residues from Nav1.7. Nav1.4 constructs were transiently expressed in HEK293 cells. The cells expressing mutant sodium channels were held at −100 mV and depolarized by a 20-ms potential of −10 mV to induce inward currents. Compared with WT Nav1.4, the N655D substitution had a negligible effect on sensitivity to 1 μM

HWTX-IV (Fig. 8*A*; 30.9 ± 2.8% inhibition, $n = 4$). However, 10 μM HWTX-IV inhibited Nav1.4 N655D currents by 75.0 ± 1.0% (Fig. 8*B*; $n = 4$), which is significantly more than the inhibition of WT Nav1.4 currents. Interestingly when the residue Gln-657 was replaced with Glu, the sensitivity of the channel to HWTX-IV was greatly increased, and 77.8 ± 2.0% of the Q657E mutant channel could be inhibited by 1 μM HWTX-IV (Fig. 8*A*; $n = 4$). Inhibition of the double mutant N655D/Q657E currents by 1 μM HWTX-IV was even greater (93.7 ± 1.0%; Fig. 8*A*). In Fig. 8*B*, Hill logistic equation fits of the dose-response curves indicated that the IC_{50} values yielded were 2.74, 0.38, and 0.13 μM on N655D, Q657E, and N655D/Q657E mutant Nav1.4 channels, respectively. The data demonstrate that the residues at positions 655 and 657 of the IIS3-S4 linker of Nav1.4 play an important role in Nav1.4 resistance to HWTX-IV.

To confirm the role of these residues in HWTX-IV inhibition, we investigated the effect of the reverse mutations in Nav1.7. The two acidic residues (Asp-816 and Glu-818) in Nav1.7, corresponding to Asn-655 and Gln-657 in Nav1.4, were replaced by Asn and Gln, respectively. Nav1.7 constructs were transiently transfected in HEK293 cells. Inward currents were induced from the mutant channels by a 20-ms depolarizing potential of −10 mV from a holding potential of −100 mV every 5 s. As with the N655D mutation in Nav1.4, the replacement of Asp-816 with Asn only slightly altered the sensitivity of Nav1.7 channel to HWTX-IV (Fig. 9*A*). The toxin at 1 μM almost completely inhibited the inward currents induced from both WT and D816N Nav1.7 channels, and the IC_{50} value for D816N (45.3 nM) was close to the value for WT channels (Fig. 9*B*). However, the E818Q substitution decreased the affinity of the toxin toward Nav1.7 channel by 63-fold with the IC_{50} value estimated to be 1.64 μM (Fig. 9*B*). Compared with the single point mutants D816N and E818Q, the double mutant D816N/E818Q channel was much more resistant to HWTX-IV. After exposure to 1 μM HWTX-IV for ~10 min, 88.5 ± 6.6% of the double mutant channel current remained available for activation. By comparison, the toxin at the same concentration inhibited Nav1.7 D816N current and E818Q current by 92.9 ± 0.6 and 37.7 ± 7.7%, respectively (Fig. 9*A*; $n = 3$). As 1 μM HWTX-IV only inhibited 11.5% of the Nav1.7 D816N/E818Q current, the IC_{50} can be roughly estimated as 7.7 μM, indicating that the double mutation reduces toxin sensitivity by at least 300-fold. These data, in conjunction with data on the Nav1.4 mutations, demonstrate that acidic residues in the IIS3-S4 linker are crucial determinants of VGSC sensitivity to HWTX-IV.

We also investigated whether differences at these residues contributed to the profound insensitivity of Nav1.5 to HWTX-IV. We replaced Arg-812 and Ser-814, the corresponding residues in hNav1.5, with Asp and Glu, respectively. Although there are multiple amino acid differences between the IIS3-S4s of Nav1.5 and Nav1.7 (Fig. 7), currents generated by the Nav1.5 R812D/S814E mutant were almost completely inhibited by 1 μM HWTX-IV (97.7 ± 0.4%, $n = 3$; Fig. 10*A*). Hill logistic equation fit of the dose-response curve (Fig. 10*B*) indicated that the IC_{50} value was 73 nM. These data confirm that the identities of the amino acids at these two positions in the IIS3-S4 linker are major determinants of the sensitivity of VGSCs to HWTX-IV.

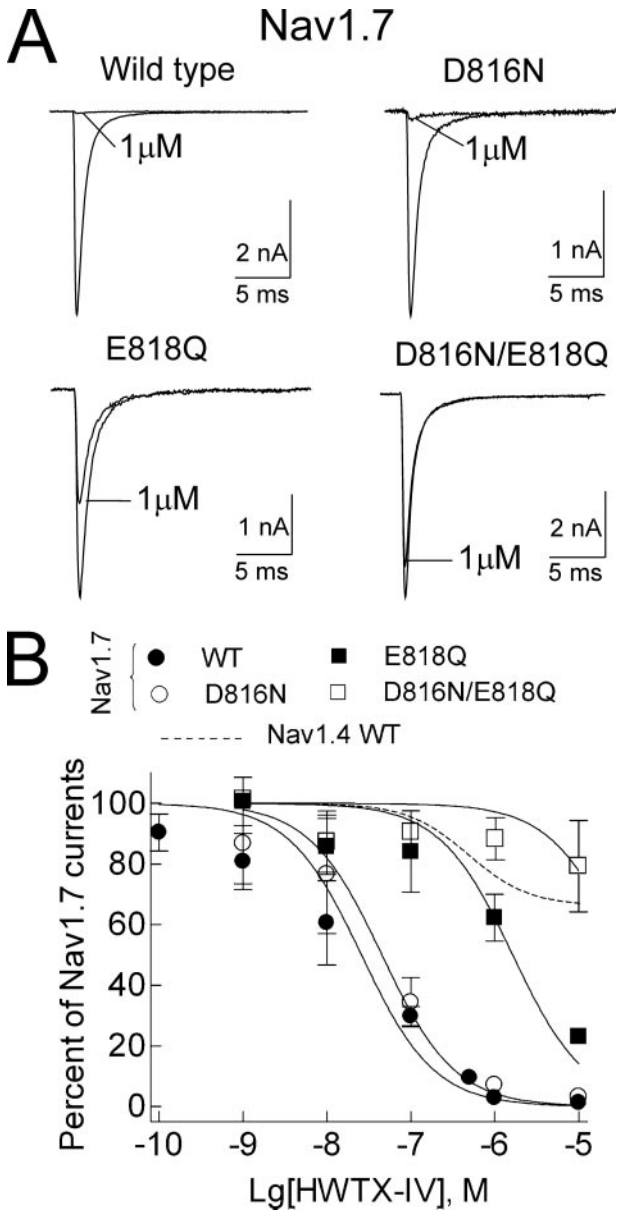

FIGURE 9. **Effects of HWTX-IV on WT and mutant Nav1.7 channels expressed in HEK293 cells.** *A*, all representative current traces recorded from WT and mutant (D816N, E818Q, and D816N/E818Q) Nav1.7 channels were elicited by a 20-ms depolarizing potential of −10 mV from a holding potential of −100 mV. The toxin concentration was 1 μM. *B*, dose-response inhibitory curves of HWTX-IV on WT and mutant Nav1.7 channels. Data points (mean ± S.E., each from three to six experimental cells) were fitted according to the Hill logistic equation. The f_{max} values for Nav1.7 D816N and E818Q channels were 0. The *dashed line* shows the fitted dose-response curve for toxin inhibition of WT Nav1.4 (see Fig. 1*F*). *Lg*, Log.

Neurotoxin receptor site 4, located at VGSC extracellular IIS3-S4 linker, is the site of interaction for scorpion β-toxins. The mechanism of the interaction for scorpion β-toxins has been suggested to involve trapping of the IIS4 voltage sensor by the toxins in the outward and activated position (12). Our site-directed mutagenesis analysis demonstrated that HWTX-IV shares the same, or an overlapping, neurotoxin receptor site with Css IV, a prototypical scorpion β-toxin from the venom of *Centruroides suffusus suffusus* (12). Therefore we asked whether the spider toxin (HWTX-IV) could also trap the IIS4 voltage sensor in an outward position. To investigate this the

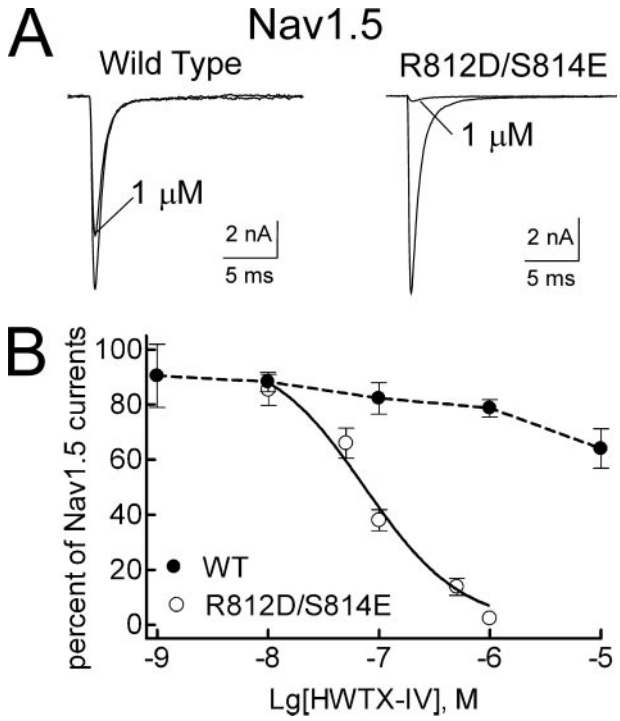

FIGURE 10. **Effects of HWTX-IV on WT and mutant Nav1.5 channels expressed in HEK293 cells.** *A*, both WT and double mutant (R812D/S814E) Nav1.5 currents were induced by a 20-ms depolarizing potential of −10 mV from a holding potential of −100 mV. The toxin concentration for treating cells was 1 μM. *B*, dose-response inhibitory curves of HWTX-IV on WT and mutant Nav1.5 channels. Data points of mutant channels (mean ± S.E., each from three to four cells) were fitted using the standard Hill equation as described under "Experimental Procedures," and the f_{max} value was 0. Data points of WT channels are connected with a *dashed line*. *Lg*, Log.

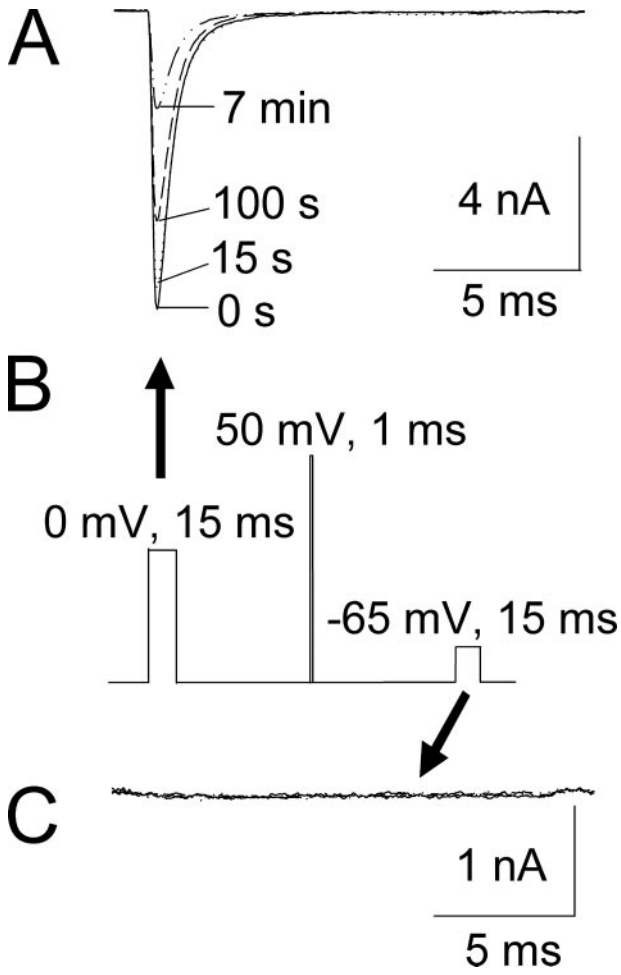

FIGURE 11. **HWTX-IV does not trap the domain II voltage sensor in an outward position.** Nav1.7 current traces in *A* and *C* were elicited by a pulse protocol as shown in *B* in which a 15-ms moderate depolarizing potential of 0 mV was applied from a holding potential of −100 mV followed 61.2 ms later by a 1-ms strong conditioning depolarizing voltage of 50 mV, and then after a second period of 61.2 ms at −100 mV, a 15-ms depolarizing potential of −65 mV was given. This protocol was applied every 5 s. *Arrows* indicate the current traces induced by moderate and strong depolarizing pulses in *B*, respectively. In *A* and *C*, the current traces 0 s, 15 s, 100 s, and 7 min after 0.1 μM toxin treatment are shown.

same protocol as described by Cestele *et al.* (12) was used to assess whether HWTX-IV might trap the IIS4 voltage sensor of the WT Nav1.7 channel in the outward position. Fig. 11*A* shows the typical current traces induced by the protocol detailed in the illustration. In the absence of toxin, the Nav1.7 channels were closed at the potentials between −80 and −60 mV (see Fig. 2*E*), and no current was recorded during a 15-ms depolarizing pulse of −65 mV from a holding potential of −100 mV. In the presence of 0.1 μM HWTX-IV, the current amplitude induced by the first test pulse (0 mV, 15 ms) was significantly depressed by 72.5% in a time-dependent manner (Fig. 11*A*; $n = 4$). However, in contrast to Css IV, which induces an inward current at −65 mV following a 1-ms conditioning depolarizing pulse of +50 mV (12), the addition of 0.1 μM HWTX-IV did not induce any substantial inward current at −65 mV (Fig. 11*C*; $n = 4$). These data, in combination with the activation data shown in Fig. 2 and the deactivation data shown in Fig. 6, demonstrate that HWTX-IV treatment does not enhance channel activation nor does it trap the voltage sensor in an outward position and indicate that the details of HWTX-IV interaction with VGSCs are distinct from that of scorpion β-toxins.

Effect of IIS3-S4 Mutations on HWTX-I Inhibition—We also examined the effect of the IIS3-S4 mutations on the sensitivity of VGSCs to HWTX-I, a 33-residue toxin from the same tarantula species that differs from HWTX-IV at 19 residues (supplemental Fig. 3) but has the same basic cysteine knot structure. HWTX-I was originally identified as a calcium channel blocker (36) but can also inhibit VGSCs (37, 38). As Fig. 12 illustrates, Nav1.7 channels were significantly more sensitive to 1 μM HWTX-I (95.7 ± 0.9% inhibition; $n = 3$) than Nav1.4 channels (5.7 ± 10.4% inhibition; $n = 3$). The Nav1.7 double mutant D816N/E818Q was only inhibited 11 ± 5% ($n = 3$) by 1 μM HWTX-I. By contrast the Nav1.4 double mutant N655D/Q657E was inhibited 95.6 ± 0.7% ($n = 3$) by 1 μM HWTX-I. Thus HWTX-I inhibition of VGSCs is also determined by the presence of specific acidic residues in the IIS3-S4 linker, and as is discussed below, this provides insight into which toxin residues might interact with the IIS3-S4 linker.

DISCUSSION

In this study, we intensively characterized the action of HWTX-IV, a 35-residue toxin from the tarantula *O. huwena* on five different VGSCs and showed that the toxin was able to inhibit neuronal subtypes Nav1.2, Nav1.3, and Nav1.7 but had little effect on skeletal muscle and cardiac isoforms Nav1.4 and

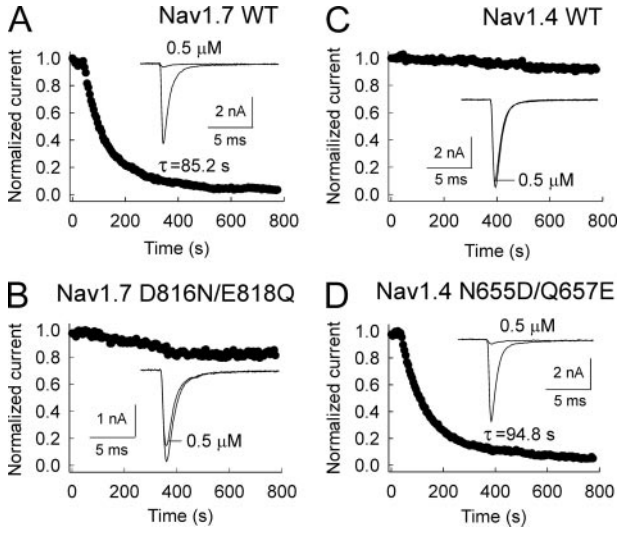

FIGURE 12. **Effects of HWTX-I on WT and mutant Nav1.4 and Nav1.7 channels transiently expressed in HEK293 cells.** Current traces (*inset*) were elicited by a 20-ms depolarizing potential of −10 mV from a holding potential of −100 mV every 5 s. *A*, WT Nav1.7; *B*, double mutant D816N/E818Q Nav1.7; *C*, WT Nav1.4; *D*, double mutant N655D/Q657E Nav1.4. The toxin concentration tested was 0.5 μM. Data are normalized to the maximum peak current amplitude. When data points in *A* and *D* were fitted by a single exponential function the time constants (*inset*) of inhibition were estimated to be ~85.2 and 94.8 s, respectively.

Nav1.5. Although HWTX-IV failed to obviously modify channel activation and steady-state inactivation in the physiological range of voltages, extreme depolarizations resulted in partial activation, and prolonged depolarizations resulted in partial recovery, indicating that the mechanism of inhibition involved voltage sensor trapping. Mutagenesis experiments showed that HWTX-IV interacts with specific residues in the IIS3-S4 linker that overlap with neurotoxin receptor site 4. However, in contrast to scorpion β-toxins, which interact with neurotoxin receptor site 4 and trap the IIS4 voltage sensor in an outward configuration, our data indicate that HWTX-IV, and the related HWTX-I, trap the IIS4 voltage sensor in a closed configuration. This is the first demonstration of neurotoxins inhibiting VGSCs by a voltage sensor trapping mechanism.

Molecular Determinants of HWTX-IV Inhibition—Our data, combined with previous data showing that HWTX-IV has no effect on TTX-resistant VGSCs on rat DRG neurons (14), indicate that HWTX-IV selectively targets neuronal TTX-sensitive VGSCs. Five TTX-sensitive VGSCs (Nav1.1–1.3, Nav1.6, and Nav1.7) are expressed in mammalian neurons. Of the VGSCs that we tested, Nav1.7 showed the highest sensitivity for HWTX-IV. This is intriguing as Nav1.7 plays crucial roles in the pathophysiology of pain (29, 39–41), and Nav1.7 blockers could aid the development of new drugs that can effectively treat pain (42). Indeed our preliminary experiments suggest that HWTX-IV can reduce pain behaviors in rats (14) (data not shown).

In our study we used site-directed mutagenesis analysis on Nav1.4 and Nav1.7 and identified two acidic residues (Asp-816 and Glu-818) in the IIS3-S4 linker that play key roles in Nav1.7 for binding HWTX-IV. The E818Q substitution decreased the affinity of Nav1.7 for HWTX-IV by 63-fold, and the double mutant Nav1.7 D816N/E818Q became almost completely resistant to HWTX-IV. Although the residue Glu-818 in Nav1.7 is conserved at the corresponding position in the HWTX-IV-sensitive VGSCs (Nav1.2 and Nav1.3), the corresponding residue is a neutral amino acid in the HWTX-IV-resistant VGSCs (Nav1.4, Nav1.5, and Nav1.8) (see Fig. 7). Of the VGSCs that we tested, the second acidic residue was only present in Nav1.7 (Asp-816), and the toxin affinity for the double mutant Nav1.4 (N655D/Q657E) increased 3-fold compared with the Q657E mutant. Therefore this second acidic residue seems to contribute to the higher sensitivity of Nav1.7 to HWTX-IV compared with the other TTX-sensitive neuronal VGSC subtypes that were tested. We did not test HWTX-IV against Nav1.1 and Nav1.6. We predict that Nav1.1, which has the glutamate corresponding to Glu-818 in Nav1.7 but not the second acidic residue in the II-S3-S4 linker, should exhibit sensitivity to HWTX-IV similar to that of Nav1.2 or Nav1.3. Nav1.6 has both acidic residues found in Nav1.7 and may also exhibit high sensitivity to HWTX-IV. However, it is predicted that HWTX-IV interacts with other residues in addition to the two that we identified as the toxin affinity was over 2-fold higher and the on-rate was 5-fold faster for Nav1.2 as compared with those for Nav1.3. Although TTX-sensitive VGSCs exhibit distinct biophysical properties (27, 43, 44), it can be difficult to distinguish between them. It may be possible to develop HWTX-IV analogs with enhanced isoform selectivity that would be useful in investigating the physiological roles of the different TTX-sensitive channels.

The IIS3-S4 linker has been identified previously as a critical part of neurotoxin receptor site 4, the receptor site for scorpion β-toxins (10). Although our data show that the IIS3-S4 linker is critical for HWTX-IV inhibition and therefore indicates that HWTX-IV belongs to the family of neurotoxin receptor site 4 toxins, the precise molecular determinants of HWTX-IV binding are different from those for other site 4 toxins. Our data predict that residue Glu-844 in Nav1.2 is crucial for HWTX-IV inhibition, but Glu-844 is not important for the action of the neurotoxin receptor site 4 scorpion β-toxin Css IV (12). Cestele *et al.* (12) determined that Gly-845 in IIS3-S4 of Nav1.2 (corresponding to Gly-819 in Nav1.7) is a crucial determinant of scorpion β-toxin binding. We did not determine whether Gly-819 is a crucial determinant of HWTX-IV binding.

Mechanism of Current Inhibition—Experiments with HWTX-IV concentrations that do not produce complete inhibition failed to identify any effect of HWTX-IV on TTX-sensitive neuronal sodium currents evoked in the physiological voltage range other than current inhibition. Thus *in vivo* HWTX-IV might be expected to behave similarly to a simple pore blocker with very slow binding kinetics. Obvious gating modifier type behavior was only observed with extreme depolarizations or very prolonged strong depolarizations (Figs. 4, 5, and 6), conditions that are unlikely to occur naturally. Therefore HWTX-IV is a gating modifier that is likely to functionally behave as a simple channel inhibitor.

Although neurotoxin receptor site 4 and the IIS3-S4 linker of VGSCs are important for the actions of scorpion β-toxins (10) and HWTX-IV, the mechanism of action of HWTX-IV is distinct from that of scorpion β-toxins. In contrast to HWTX-IV, anti-mammalian scorpion β-toxins are excitatory toxins and

cause a hyperpolarizing shift in the voltage dependence of VGSC activation (12). Several studies have shown that strong depolarizations are needed to induce the scorpion β-toxin modification of the voltage dependence of activation and that the modulatory action can be reversed by strong hyperpolarization (12, 45), suggesting that scorpion β-toxin action is dependent on voltage-induced changes in channel conformation. The S4 segments, with their positively charged residues, are crucial components of the voltage sensors of VGSCs, and the S4s of domains I–III are specifically related to channel activation (46). The modification of activation by scorpion β-toxins has been explained using a voltage sensor trapping model in which scorpion β-toxins trap the VGSC voltage sensor of domain II in an open, or outward, configuration. In contrast, scorpion α-toxins and sea anemone toxins inhibit sodium current inactivation by binding at the extracellular IVS3-S4 linker (receptor site 3) and likely trap the IVS4 segment in the closed configuration (11). Strong depolarization can accelerate the dissociation of scorpion α-toxin·channel complexes. Similar to scorpion α-toxin Lqh-II, the complex HWTX-IV·Nav1.7 can be separated by strong depolarizations, but it seems that HWTX-IV binding is much stronger. After Nav1.7 channel was blocked by 1 μM HWTX-IV, we did not observe any dissociation of the toxin·channel complex following a 500-ms conditioning pulse at +30 or +100 mV. By comparison, the time constant for dissociation of α-toxin Lqh-II from Nav1.2 channels at +100 mV is around 100 ms (47). A 5-min conditioning pulse at +30 mV allowed partial recovery from HWTX-IV inhibition (Fig. 5*D*), indicating that the time constant for recovery of Nav1.7 channels at +30 mV from HWTX-IV block is on the order of 400 s. Even at +150 mV the estimated time constant for recovery of Nav1.7 from HWTX-IV block was ~8 s. This is much slower than recovery of Kv2.1 channels from inhibition by hanatoxin, a Kv2.1 gating modifier purified from the venom of the tarantula *Grammostola spatulata* (48). The time constant for recovery of Kv2.1 channels from hanatoxin at +80 mV is 261 ms (33). In contrast to scorpion β-toxins, hanatoxin stabilizes the resting conformation of the potassium channel voltage sensor and shifts the voltage dependence of activation in the depolarizing direction by ~50 mV (30). Our data suggest that HWTX-IV shifts the voltage dependence of activation of Nav1.7 channels by more than +200 mV (see Fig. 4). The exact magnitude of this shift is difficult to estimate with channels that exhibit rapid inactivation. Unfortunately inactivation-deficient Nav1.7 channels are difficult to express in HEK293 cells.[4] Nonetheless these data indicate that HWTX-IV is likely to inhibit VGSC activation by tightly binding at (or overlapping with) neurotoxin receptor site 4 and trapping IIS4 in the closed configuration.

Based on this proposed mechanism of action, HWTX-IV should block the gating charge associated with the voltage sensor in domain II. Although gating currents have been recorded for Nav1.4 and Nav1.5 channels expressed in HEK293 cells (49, 50), very high channel densities are needed. Unfortunately in our experience the channel density achieved with Nav1.7 and other neuronal isoforms is typically one-tenth that achieved with the muscle isoforms, and therefore Nav1.7 gating current measurements were not feasible in HEK293 cells. Recently Campos *et al.* (51) used the cut-open oocyte preparation and elegant spectroscopic measurements to definitively show that β-scorpion toxins do indeed immobilize the voltage sensor of domain II and reduce the total gating current by ~20%. Based on these data we expect that HWTX-IV also reduces the total gating charge by ~20%.

Comparison with Other Peptide Toxins That Interact with Ion Channels—Several spider toxins slow VGSC inactivation in a similar manner to scorpion α-toxins and likely bind to neurotoxin receptor site 3 (13). Although these toxins may trap the IV-S4 in the closed configuration, they impair inactivation and are excitatory. ProTx-II, from the venom of the tarantula *Thrixopelma pruriens*, has been shown to inhibit sodium currents, but in contrast to HWTX-IV, ProTx-II obviously modifies the voltage dependence of VGSC activation in the physiological voltage range (22). It also had been proposed that ProTx-II might interact with neurotoxin receptor site 4 (52). However, using extensive mutagenesis of Nav1.5, Smith *et al.* (24) recently showed that this may not be the case. ProTx-II does not apparently target other known receptor sites, suggesting the existence of a novel toxin binding site coupled to activation. Several tarantula toxins have been identified that inhibit activation of potassium channels by interacting with S3-S4 linkers (31). Potassium channels can be formed by four identical subunits, and although it seems that multiple toxin molecules can simultaneously bind a potassium channel it also seems that binding of only one toxin molecule per potassium channel is needed to produce channel inhibition (31). Our mutagenesis data indicate that binding of one HWTX-IV molecule per channel is sufficient and necessary for VGSC inhibition. Our data with subsaturating concentrations (Figs. 2 and 3) demonstrated that HWTX-IV does not have multiple actions and therefore is unlikely to interact with multiple S4s.

We also showed that the acidic residues in IIS3-S4 are important for the actions of both HWTX-IV and HWTX-I. Although HWTX-IV and HWTX-I share a common cysteine knot structure, only 14 of the 35 residues (including the six cysteines) in HWTX-I are conserved in HWTX-IV (supplemental Fig. 3). Li *et al.* (8) demonstrated that alanine replacement of Lys-27 and Arg-29 in hainantoxin-IV, another tarantula toxin that seems to selectively target TTX-sensitive VGSCs (53), reduces the toxin binding affinity by 2 orders of magnitude. Because positively charged residues are conserved at the same positions in HWTX-I and HWTX-IV, but not in ProTx-II, we predict that these basic residues play crucial roles in high affinity binding of HWTX-I and HWTX-IV to IIS3-S4 of VGSCs. Interestingly HWTX-I also seems to inhibit N-type calcium channels (36), although the molecular determinants of this interaction are not known, and it is not clear whether this calcium channel inhibition might involve S4 segment trapping. Acidic residues in S3-S4 linkers are important determinants of ω-agatoxin-IVA binding to P-type calcium channels (34) and hanatoxin binding to Kv1.2 potassium channels (54). Our data support the proposal that there is a conserved binding mechanism for gating

[4] T. R. Cummins, unpublished observations

modifier toxins that inhibit the activation of voltage-gated ion channels (34).

Overall our findings provide novel mechanistic insight into how tarantula toxins can inhibit VGSCs. This is the first demonstration of a VGSC inhibitor binding to an S4 segment. This raises the possibility that other agents that inhibit VGSCs by trapping the S4 segments of domain I, II, or III in closed configurations might be discovered or developed. Because peptide toxins are likely to interact with multiple residues on VGSCs, it might be possible to identify or develop peptides with increased isoform-specific selectivity, and these could be invaluable for investigating the localization and physiological roles of VGSCs.

REFERENCES

1. Catterall, W. A., Goldin, A. L., and Waxman, S. G. (2005) *Pharmacol. Rev.* **57,** 397–409
2. Goldin, A. L., Barchi, R. L., Caldwell, J. H., Hofmann, F., Howe, J. R., Hunter, J. C., Kallen, R. G., Mandel, G., Meisler, M. H., Netter, Y. B., Noda, M., Tamkun, M. M., Waxman, S. G., Wood, J. N., and Catterall, W. A. (2000) *Neuron* **28,** 365–368
3. Zhu, S., Bosmans, F., and Tytgat, J. (2004) *J. Mol. Evol.* **58,** 145–153
4. Catterall, W. A. (2000) *Neuron* **26,** 13–25
5. Ogata, N., and Tatebayashi, H. (1993) *J. Physiol.* **466,** 9–37
6. Shon, K. J., Olivera, B. M., Watkins, M., Jacobsen, R. B., Gray, W. R., Floresca, C. Z., Cruz, L. J., Hillyard, D. R., Brink, A., Terlau, H., and Yoshikami, D. (1998) *J. Neurosci.* **18,** 4473–4481
7. Cummins, T. R., Aglieco, F., and Dib-Hajj, S. D. (2002) *Mol. Pharmacol.* **61,** 1192–1201
8. Li, D., Xiao, Y., Hu, W., Xie, J., Bosmans, F., Tytgat, J., and Liang, S. (2003) *FEBS Lett.* **555,** 616–622
9. Escoubas, P., Diochot, S., and Corzo, G. (2000) *Biochimie* (*Paris*) **82,** 893–907
10. Cestele, S., and Catterall, W. A. (2000) *Biochimie* (*Paris*) **82,** 883–892
11. Rogers, J. C., Qu, Y., Tanada, T. N., Scheuer, T., and Catterall, W. A. (1996) *J. Biol. Chem.* **271,** 15950–15962
12. Cestele, S., Qu, Y., Rogers, J. C., Rochat, H., Scheuer, T., and Catterall, W. A. (1998) *Neuron* **21,** 919–931
13. Xiao, Y., Tang, J., Hu, W., Xie, J., Maertens, C., Tytgat, J., and Liang, S. (2005) *J. Biol. Chem.* **280,** 12069–12076
14. Peng, K., Shu, Q., Liu, Z., and Liang, S. (2002) *J. Biol. Chem.* **277,** 47564–47571
15. Liang, S. P., Zhang, D. Y., Pan, X., Chen, Q., and Zhou, P. A. (1993) *Toxicon* **31,** 969–978
16. Kearney, J. A., Plummer, N. W., Smith, M. R., Kapur, J., Cummins, T. R., Waxman, S. G., Goldin, A. L., and Meisler, M. H. (2001) *Neuroscience* **102,** 307–317
17. Cummins, T. R., Aglieco, F., Renganathan, M., Herzog, R. I., Dib-Hajj, S. D., and Waxman, S. G. (2001) *J. Neurosci.* **21,** 5952–5961
18. Ukomadu, C., Zhou, J., Sigworth, F. J., and Agnew, W. S. (1992) *Neuron* **8,** 663–676
19. Klugbauer, N., Lacinova, L., Flockerzi, V., and Hofmann, F. (1995) *EMBO J.* **14,** 1084–1090
20. Lossin, C., Wang, D. W., Rhodes, T. H., Vanoye, C. G., and George, A. L., Jr. (2002) *Neuron* **34,** 877–884
21. Corzo, G., Sabo, J. K., Bosmans, F., Billen, B., Villegas, E., Tytgat, J., and Norton, R. S. (2007) *J. Biol. Chem.* **282,** 4643–4652
22. Middleton, R. E., Warren, V. A., Kraus, R. L., Hwang, J. C., Liu, C. J., Dai, G., Brochu, R. M., Kohler, M. G., Gao, Y. D., Garsky, V. M., Bogusky, M. J., Mehl, J. T., Cohen, C. J., and Smith, M. M. (2002) *Biochemistry* **41,** 14734–14747
23. Nicholson, G. M., Walsh, R., Little, M. J., and Tyler, M. I. (1998) *Pfluegers Arch. Eur. J. Physiol.* **436,** 117–126
24. Smith, J. J., Cummins, T. R., Alphy, S., and Blumenthal, K. M. (2007) *J. Biol. Chem.* **282,** 12687–12697
25. Szeto, T. H., Birinyi-Strachan, L. C., Smith, R., Connor, M., Christie, M. J., King, G. F., and Nicholson, G. M. (2000) *FEBS Lett.* **470,** 293–299
26. Bosmans, F., Rash, L., Zhu, S., Diochot, S., Lazdunski, M., Escoubas, P., and Tytgat, J. (2006) *Mol. Pharmacol.* **69,** 419–429
27. Herzog, R. I., Cummins, T. R., Ghassemi, F., Dib-Hajj, S. D., and Waxman, S. G. (2003) *J. Physiol.* **551,** 741–750
28. Matavel, A., Cruz, J. S., Penaforte, C. L., Araujo, D. A., Kalapothakis, E., Prado, V. F., Diniz, C. R., Cordeiro, M. N., and Beirao, P. S. (2002) *FEBS Lett.* **523,** 219–223
29. Lee, H. C., Wang, J. M., and Swartz, K. J. (2003) *Neuron* **40,** 527–536
30. McDonough, S. I., Lampe, R. A., Keith, R. A., and Bean, B. P. (1997) *Mol. Pharmacol.* **52,** 1095–1104
31. Swartz, K. J. (2007) *Toxicon* **49,** 213–230
32. Huang, C. J., and Moczydlowski, E. (2001) *Biophys. J.* **80,** 1262–1279
33. Phillips, L. R., Milescu, M., Li-Smerin, Y., Mindell, J. A., Kim, J. I., and Swartz, K. J. (2005) *Nature* **436,** 857–860
34. Winterfield, J. R., and Swartz, K. J. (2000) *J. Gen. Physiol.* **116,** 637–644
35. Saab, C. Y., Cummins, T. R., Dib-Hajj, S. D., and Waxman, S. G. (2002) *Neurosci. Lett.* **331,** 79–82
36. Peng, K., Chen, X. D., and Liang, S. P. (2001) *Toxicon* **39,** 491–498
37. Cummins, T. R., Moczydlowski, E., and Bingham, J. P. (2004) *Society for Neuroscience Annual Meeting, San Diego, October 23–27, 2004*, Abstr. 398.4, Society for Neuroscience, Washington, DC
38. Wang, M., Guan, X., and Liang, S. (2007) *Biochem. Biophys. Res. Commun.* **357,** 579–583
39. Cox, J. J., Reimann, F., Nicholas, A. K., Thornton, G., Roberts, E., Springell, K., Karbani, G., Jafri, H., Mannan, J., Raashid, Y., Al-Gazali, L., Hamamy, H., Valente, E. M., Gorman, S., Williams, R., McHale, D. P., Wood, J. N., Gribble, F. M., and Woods, C. G. (2006) *Nature* **444,** 894–898
40. Dib-Hajj, S. D., Cummins, T. R., Black, J. A., and Waxman, S. G. (2007) *Trends Neurosci.* **30,** 555–563
41. Sheets, P. L., Jackson, J. O., II, Waxman, S. G., Dib-Hajj, S. D., and Cummins, T. R. (2007) *J. Physiol.* **581,** 1019–1031
42. Cummins, T. R., and Rush, A. M. (2007) *Expert Rev. Neurother.* **7,** 1597–1612
43. Cummins, T. R., Howe, J. R., and Waxman, S. G. (1998) *J. Neurosci.* **18,** 9607–9619
44. Rush, A. M., Cummins, T. R., and Waxman, S. G. (2007) *J. Physiol.* **579,** 1–14
45. Mantegazza, M., and Cestele, S. (2005) *J. Physiol.* **568,** 13–30
46. Chanda, B., and Bezanilla, F. (2002) *J. Gen. Physiol.* **120,** 629–645
47. Gilles, N., Leipold, E., Chen, H., Heinemann, S. H., and Gordon, D. (2001) *Biochemistry* **40,** 14576–14584
48. Swartz, K. J., and MacKinnon, R. (1995) *Neuron* **15,** 941–949
49. Bendahhou, S., Cummins, T. R., and Agnew, W. S. (1997) *Am. J. Physiol.* **272,** C592–C600
50. Sheets, M. F., and Hanck, D. A. (1999) *J. Physiol.* **514,** 425–436
51. Campos, F. V., Chanda, B., Beirao, P. S., and Bezanilla, F. (2007) *J. Gen. Physiol.* **130,** 257–268
52. Smith, J. J., Alphy, S., Seibert, A. L., and Blumenthal, K. M. (2005) *J. Biol. Chem.* **280,** 11127–11133
53. Xiao, Y., and Liang, S. (2003) *Eur. J. Pharmacol.* **477,** 1–7
54. Li-Smerin, Y., and Swartz, K. J. (2000) *J. Gen. Physiol.* **115,** 673–684